Indian Journal of Chemistry
Vol. 60A, April 2021, pp. 506-518

New mono- and polynuclear copper(II) complexes: Structural characterization, quantum chemical calculations and antioxidant superoxide dismutase studies

Ram N Patel[a,*], Satish K Patel[a,*], D Kumhar[a], Nirmala Patel[b] & Raymond J Butcher[c]

[a]Department of Chemistry, A.P.S. University, Rewa, Madhya Pradesh 486 003, India

[b]Department of Botany, Govt. Science College, Rewa, Madhya Pradesh 486 003, India

[c]Department of Inorganic and Structural Chemistry, Howard University, Washington DC 22031, USA

*E-mail: patelsatish33@yahoo.co.in (SKP)/ rnp64@ymail.com (RNP)

Received 02 November 2020; revised and accepted 15 February 2021

Two copper(II) complexes have been synthesized and characterized using elemental and spectral analysis. The molecular structures of both complexes have been confirmed by single crystal X-ray analysis. The stability of the metal centre was examined using cyclic and differential pulse voltammetry in DMSO solution. X-band electron paramagnetic spectra were recorded both in solid and frozen solution to confirm the d^9 configuration. Frozen solution spectra of complexes have the trend in the spin Hamiltonian parameters $g_{\parallel} > g_{\perp} > 2.0023$ and $A_{\parallel} \simeq 156 \times 10^{-4}$ cm^{-1} revealing a $d_{x^2-y^2}$ ground state with tetragonal symmetry for copper(II) ion. Density functional calculations have been performed and results are found to agree with the experimental results. Antibacterial activities of complexes were screened by taking gram-positive and gram-negative bacteria. Further, *in vitro* antioxidant (superoxide dismutase) properties of **1** and **2** showed considerable activity compared to other SOD mimics.

Keywords: Single crystal X-ray, Cu(II) complex, Superoxide dismutase, Hirshfeld analysis, Biological activity

Copper is one of the essential member in varied biological processes and its importance in both enzymatic[1] and non-enzymatic[2] chemical systems is well established. One such enzyme is superoxide dismutase (SOD). This enzyme serves a vital role in defending oxygen-utilizing life forms from oxidative damage[3]. All mammalian life utilizes molecular oxygen as the ultimate oxidant during cellular respiration during which one electron reduction product, superoxide anion (O_2^-) is released. This deleterious oxygen-derived free radical has been demonstrated to be a mediator of reperfusion diseases, such as acute mitochondrial stroke, shown to be associated with the development and contamination of inflammatory processes. This is involved in many diseases such as arthritis and plays a major role in the initiation of neurological disorders such as Parkinson's disease. The rational design and synthesis of low molecular weight copper(II) complexes that mimic a natural enzyme function possess a potential for use as a human pharmaceutical in the prevention of such diseases. Such oxidative enzyme SOD control the overproduction of toxic O_2^- by dismutation processes into molecular oxygen and hydrogen peroxide (Eqns 1 and 2).

$$O_2^- + M^{n+1} \rightarrow O_2 + M^n \quad \ldots (1)$$

$$M^n + O_2^- \rightarrow H_2O_2 + M^{n+1} \quad \ldots (2)$$

In light of chemical data surrounding the use of the SOD enzymes[4], the low molecular weight of the enzyme SOD has been proposed for the treatment of several diseases. In fact, we are interested in the synthesis of low molecular weight complexes as a structural and functional model for SOD mimics using Di(2-picolyl)amine and pyrazine. With these views in mind, in the present article two new copper(II) mono- and polynuclear complexes $[Cu(DPA)_4](ClO_4)_2$ (**1**) and $[Cu_2(\mu\text{-pyrz})(pyrz)_3](ClO_4)_4$ (**2**) have been synthesized and characterized using various physico-chemical techniques. Molecular structures of these newly synthesized complexes were determined using single crystal X-ray analysis. Experimental bond angles and bond distances were also compared with theoretical data generated by quantum chemical calculations. We have explored their performance

in-vitro as SOD mimics using nitro blue tetrazolium chloride (NBT) assay method.

Materials and Methods

All used reagents and chemicals were of reagent grade. Di-(2-picolyl)amine, pyrazine and copper(II) perchlorate hexahydrate[#] were purchased from Across Organics and used without further purification.

Synthesis of $[Cu(DPA)_4](ClO_4)_2$ (1)

Copper perchlorate hexahydrate (0.370 g, 1 mmol) was added to 20 mL methanol. After 30 min, Di-(2-picolyl)amine (0.8 mL, 1 mmol) added and stirred for 3 h at room temperature. The obtained solution was left undisturbed for few days for evaporation at ambient temperature to get blue crystals. These crystals were washed with ether and finally dried over calcium chloride in a desiccator. Yield: (~73%). Anal (%) Calcd (Found) for $C_{48}H_{51}Cl_4Cu_2N_{12}O_{16}$ (M. W. = 1320.89 g mol^{-1}): C, 43.64 (43.78); H, 3.89 (3.83); N, 12.72 (12.64). Conductance (DMSO); Λ_m = 235 S cm^2 mol^{-1}. Electronic absorption spectrum (DMSO); λ_{max} ~652 nm and ε = 403 M^{-1} cm^{-1}, FT-IR bands (KBr, cm^{-1}): υ(C=N) 1573, υ(C=O) 1610, υ(ClO_4^-) 1086 (Supplementary Data, Fig. S1).

Synthesis of $[Cu_2(\mu\text{-pyrz})(pyrz)_3](ClO_4)_4$ (2)

20 mL methanol solution of copper(II) perchlorate hexahydrate (0.370 g, 1 mmol) was constantly stirred for 20 min and after that pyrazine (0.040 g, 0.5 mmol) was added in a dropwise manner. The obtained green solution was left undisturbed for few days to evaporate at ambient temperature to obtain blue crystals. The crystals were collected by filtration and dried over calcium chloride desiccator. Yield: (~73%). Anal (%) Calcd (Found) for $C_9H_8ClCuN_6O_4$ (M. W. = 830.53 g/mol): C, 29.76 (29.82); H, 2.22 (2.17); N, 23.13 (23.01). Conductance (DMSO); Λ_m = 211 S cm^2 mol^{-1}. Electronic absorption spectrum (DMSO); λ_{max} = 620 nm and ε = 133 M^{-1} cm^{-1}, FT-IR bands (KBr, cm^{-1}): υ(C=N) 1626, υ(C=O) 1537, υ(ClO_4^-) 1086 (Supplementary Data, Fig. S1).

Characterization techniques

Elemental analyses were performed at SAIF, CDRI, Lucknow. The UV-visible absorption spectra were recorded on a Shimadzu UV-1601 spectrophotometer. The Fourier transform infrared (FTIR) spectral data were obtained on a Perkin-Elmer IR α-T Spectrophotometer. The electron paramagnetic resonance (epr) spectra of copper(II) complexes in solid and solutions were recorded with a Varian E-line Century Series Spectrometer operating at X-band (9.25 G Hz) modulation frequency at room and low temperatures. The electrochemical behaviours of complexes were collected with the help of cyclic voltammetry (CV) and differential pulse voltammetry (DPV) measurements under a dry nitrogen atmosphere. Ag/AgCl electrode was used as the reference electrode and ferrocene-ferrocenium couple as an internal standard in cyclic voltammetry[5].

X-ray crystallographic studies

The crystals suitable for single crystal X-ray diffraction studies were obtained by slow cooling of methanol solutions containing **1** and **2**. The diffraction data were collected at 298 K using Bruker D8 Venture diffractometer equipped with graphite monochromated Mo-Kα radiation. The intensity data of both complexes were corrected for absorption. All non-hydrogen atoms were refined with anisotropic thermal parameters. Both structures were solved by direct method[6] and refined on F2 by a full-matrix least-squares procedure using anisotropic displacement parameters.[7] All geometrical calculations were performed using PLATON[8] and WINGX[9] programs. The hydrogen atom positions bonded to carbon atoms were initially estimated by geometry with anisotropic displacement data. The molecular structures were solved by SHELXS 97[10] and refined on F^2 full-matrix least square procedure.

Antibacterial activity measurements

Antibacterial activities of the complexes were evaluated using the diffusion disk method[11]. The details of this technique was followed from the published work[12].

SOD activity measurements

Inhibition of superoxide anion radical anion (O_2^-) formation by alkaline DMSO (NBT assay) was evaluated according to the previously reported procedures[13]. In the presence as well as the absence of the complexes the O_2^- was generated in situ by alkaline DMSO and NBT reduction to MF^+ by O_2^- was monitored spectrophotometrically at 560 nm in phosphate buffer. A unit of antioxidant SOD activity is the concentration of the complex, which causes 50% (IC_{50}) inhibition of alkaline DMSO and mediated reduction of NBT. Two assays were performed for each concentration of metal complexes. The catalytic

[#]**Caution!** Although no problems were encountered during the synthesis of copper(II) complexes, perchlorate salts are potentially explosive and handled with extreme care.

rate constants were calculated[14] as $K_{M_CCF} = K_{NBT}$ [NBT]/IC_{50}, where K_{NBT}(pH 7.8) = 5.94 × M^{-1} S^{-1}.

Computational method

Theoretical calculations were performed regarding molecular structure optimization and HOMO-LUMO energies etc. of complexes **1** and **2**. Full geometry optimizations were carried out using the density functional theory (DFT) method at the B3LYP level for the complex.[15] All DFT calculations were carried out starting from the experimental single crystal X-ray data as input geometries. The geometry optimizations of both complexes were carried out in the gas using Gaussion 9 software package. All elements except Cu were assigned the LANL2DZ basis set.[16] LANL2DZ with effective core potential for Cu atom was used[17]. In the computational model, the cationic complex was taken into account. All calculations were performed with the GAUSSIAN09 program,[18] with the aid of the Gauss View visualization program. Vertical electronic excitations based on B3LYP optimized geometries were evaluated using the time-dependent density functional theory (TDDFT) formalism[19] in DMSO, using a conductor-like polarizable continuum model.[20]

Results and Discussion

Two new copper complexes were prepared by the reaction of tridentate Schiff base (HL) and copper(II) salt in methanol. The synthetic routes of complexes are shown in Scheme 1. All kinds of general characterizations were carried out with polycrystalline samples. The microanalyses data for both the complexes were found to be consistent with their corresponding chemical compositions. Both complexes were air stable and soluble in DMSO and DMF. The FTIR data of both complexes show absorption band resulting from the skeleton vibration of the aromatic rings in the region of 1390-1630 cm^{-1}. The splitting of band ~1085 cm^{-1} indicates the coordinated perchlorate ion in **1**[21].

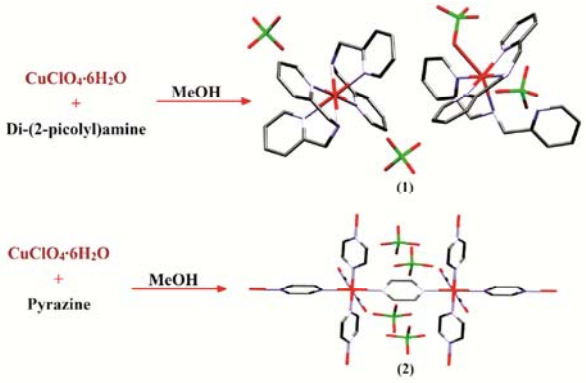

Scheme 1 — Synthetic route of complexes **1** and **2**

In both complexes, the presence of bands at 1090, 1092, 622 and 619 cm^{-1} indicate a tetrahedral symmetry of perchlorate ion. This, therefore, suggest the presence of perchlorate outside the coordination sphere[22]. The coordination of ligands is substantiated by a band due to υ(M-N/O) in the range of ~440-525 cm^{-1}.[23]

Description of structures

Crystallographic data, refinement parameters, bond distances and bond angles for both the complexes are given in Table 1 and in Supplementary Data,

Table 1 — Crystal data and structure refinement parameters of synthesized complexes **1** and **2**

Parameter	**1**	**2**
Empirical formula	$C_{48}H_{51}Cl_4Cu_2N_{12}O_{16}$	$C_9H_8ClCuN_6O_4$
Formula weight	1320.89	363.20
Temperature (K)	100(2)	100(2)
Wavelength (Å)	0.71073	0.71073
Crystal system	Monoclinic	Tetragonal
Space group	*P 21/n*	*P 4/n b m*
a (Å)	23.1720(9)	9.779(16)
b (Å)	9.2985(3)	9.779(16)
c (Å)	25.5553(10)	6.786(11)
α (°)	90	90
β (°)	95.481(2)	90
γ (°)	90	90
Volume ($Å^3$)	5481.1(4)	649(2)
Z	4	2
Density (calculated) (Mg/m^3)	1.601	1.859
Absorption coefficient (mm^{-1})	1.052	1.915
F(000)	2708	364
Theta range for data collection (°)	2.521 to 28.368	2.946 to 30.746
Index ranges	-30<=h<=30, -12<=k<=12, -34<=l<=34	-11<=h<=13, -8<=k<=12, -6<=l<=9
Reflections collected	78937	1122
Independent reflections	13683 [R(int) = 0.0527]	483 [R(int) = 0.0819]
Completeness to theta = 25.242°	99.9 %	94.2 %
Absorption correction	None	None
Refinement method	Full-matrix least-squares on F^2	Full-matrix least-squares on F^2
Data / restraints / parameters	13683 / 138 / 824	483 / 0 / 30
Goodness-of-fit on F^2	1.064	1.154
Final R indices [I>2sigma(I)]	R1 = 0.0455, wR2 = 0.1002	R1 = 0.0982, wR2 = 0.2317
R indices (all data)	R1 = 0.0809, wR2 = 0.1233	R1 = 0.1274, wR2 = 0.2459
Extinction coefficient	n/a	n/a
Largest diff. peak and hole (e.$Å^{-3}$)	1.122 and -0.833	1.388 and -0.915

Table S1. Crystal structure of the mononuclear complex, **1** consists of two $[Cu(HL)_2]^{2+}$ species along with four perchlorate molecules. Molecular structure, coordination sphere, partial packing diagram (dimer of dimer model), H-bondings with atom numbering scheme and packing diagram along with *b*-axis for compex **1** are given in Fig. 1. The species consists of a copper ion and tridentate ligand in one whereas in another species one copper ion, one tridentate ligand and one perchlorate anion weakly coordinated to copper ion (Cu-O = 2.774 Å). The coordination geometry around the copper ion is best described as a distorted octahedral geometry. The least-square plane constituted by four equatorially coordinated atoms reveals appreciable distortions with the maximum atomic deviations of 0.021 Å and 0.030 Å. The distortion in geometry from ideal octahedral is also expressed by the difference in the range of *cisoid* angles [78.79(9)-96.90(11) and 79.67(12)-101.36(10)] and *transoid* angles [159.58-178.02(11) and 176.11(10)-179.80(12)], which deviate from the ideal angle of 90° and 180°, respectively. Furthermore, axial distances Cu(1)-N(3A) and Cu(1)-O(41) = 2.354(2) and Cu(1)-O(41) in one cationic unit and Cu(1)-N(5B) and Cu(2)-N(1B) in the second unit are markedly longer than the average Cu-N distances (≅2.0 Å).

The hexa-aqua copper cation is sitting on a crystallographic center of symmetry. One interesting feature of the crystal structure of complex **1** is that the stability of this structure is assumed to be due to the four perchlorate counter ions which stabilize the whole system by strong H-bonding network systematically distributed throughout the lattice (Fig. 1b). The extended network of H-bonding is constructed through the perchlorate molecules and hydrogen atoms of tridentate HL. The hydrogen atom of HL C5AA-H5AA forms trifurcated H-bonding with Cl3, O32 and O33 atoms. Similarly, H-atom of C24A-H24A also forms bifurcated H-bondings with Cl2 and O22 and C12B-H12B yields H-bonding with O21 and Cl2, $R_2^1(3)$. Two large synthons are formed by C2B-H2BA and C3B-H3BA H-atoms with two O atoms of perchlorate O32 and O33, $R_2^2(7)$. O31 atom

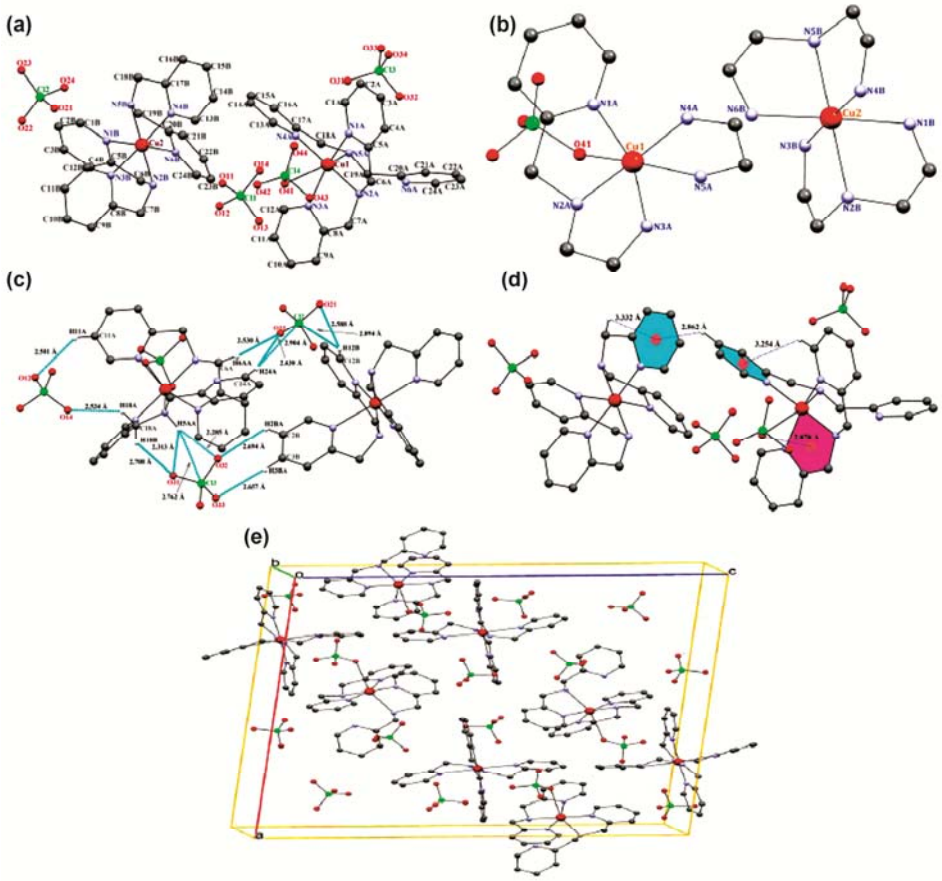

Fig. 1 — (a) Molecular structure, (b) coordination sphere, (c) partial packing diagram (dimer of dimer model), (d) H-bondings with atom numbering scheme, and (e) Packing diagram along with *b*-axis of complex **1**

of this perchlorate atom also involves in formation of heterosynthon, $R_2^1(5)$ with H-atoms of C5AA-H5AA and C18A-H18B, all kinds of H-bonding parameters are presented in Supplementary Data, Table S2. Hydrogen atoms of H18C and H15A attached to C18B and C15A are involved in the intermolecular C-H$\cdots\pi$ interactions with phenyl ring, C13B, C14B, C15B, C16B, C17B and N4B (cg1). Similarly, H1AA attached to C1A is involved in intermolecular C-H$\cdots\pi$ interactions with phenyl ring, C13, C14B, C15B, C16B, C17B and N4B (cg2). In addition, to these C-H$\cdots\pi$ interactions, one anion intramolecular π interaction with chelate ring is observed. The O41 attached to Cl4 is involved in Cl4-O41$\cdots\pi$ (metal chelate) ring, Cu1, N2A, N3A, C7A and C8A (Fig. 1c). In this complex, the ring centroid (H/O$\cdots$cg) distances are in the range of 332-2.862 Å. The C-H$\cdots$cg(1/2), angles remain in the range 3.332-3.254 Å are still below the optimum value (180º) for strongest C-H$\cdots\pi$ interactions, which may be due to the steric constraints in the molecule. Such type of inter and intra C-H$\cdots\pi$ interactions are responsible for extra stabilization of complex in its solid state. A view of the unit cell along the b-axis is shown in Fig. 1d. It can be seen that the molecules are packed in a two-dimensional manner with a parallel arrangement of rings.

The single crystal X-ray analysis of complex **2** shows that the complex exists a pyrazine bridged polymers. The molecular structure, coordination sphere, Partial packing diagram (dimer of dimer model), lp $-\pi$(aryl) centroid interactions and packing diagram along *a*-axis of complex **2** are shown in Fig. 2. The molecule is centrosymmetric with c_1 symmetry, the centre of symmetry being located at the copper central metal. The coordination sphere around the copper(II) center can be described as octahedral, having CuN6 chromophore. In this complex, the equatorial positions are occupied by two pyrazine nitrogen atoms (N2). The bond distances in the equatorial are 2.058 Å. Axial distances (Cu-N) are

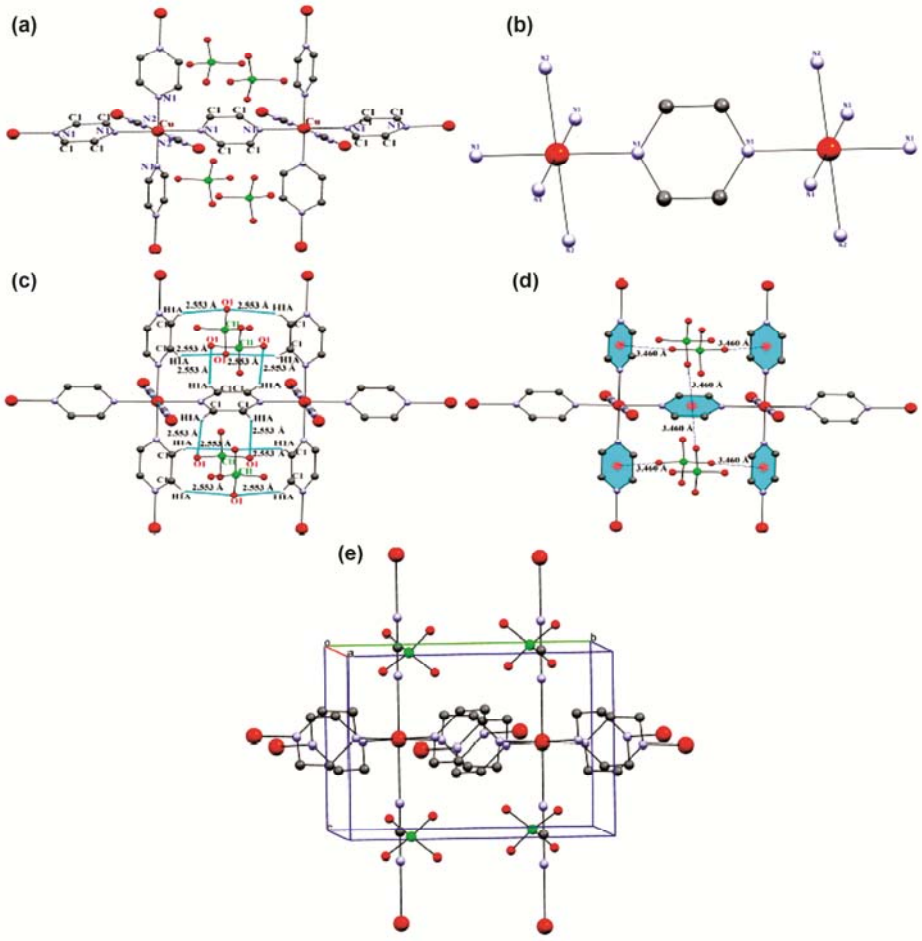

Fig. 2 — (a) Molecular structure, (b) coordination sphere, (c) partial packing diagram (dimer of dimer model), (d) lp $-\pi$(aryl) centroid interactions, and (e) Packing diagram along *a*-axis of complex **2**

2.333 Å. The axial Cu-N distances are elongated due to Jahn-Teller distortion.[24] In this complex all the cisoid angles are 90 and transoid angles are 180°. Therefore, the coordination geometry of each copper centre is best described as axially elongated ideal octahedral.[25] In this complex H-bonding is constructed through H-atoms of phenyl ring of HL and O atoms of perchlorate anions (Fig. 2b). In this complex anion beside these H-bondings, anion-π interaction is present in **2** (Fig. 2c). The O atoms of perchlorate anion remain perfectly centered on the coordinate pyrazine ring (angle to O···centroid 90°. Similar anion···π interactions in copper(II) complexes are reported.[26] Anion···π interactions are quite versatile and should be of general importance for the solid state structures and supramolecular assembly.

Epr spectra

Epr spectra of both complexes were recorded for a polycrystalline sample at room temperature (RT) and in DMSO solutions (3×10^{-3} M) at LNT are shown in Fig. 3. Polycrystalline spectrum at RT shows hyperfine splitting (anisotropic) with $g_{\parallel} = 2.14$ and $g_{\perp} = 2.064$. A very weak signal at a low magnetic field ($g_e = 4.0$) due to a singlet-triplet transition ($\triangle M_s = \pm 2$) is present. Such observation is in agreement with the antiferromagnetic interaction between a copper ion in solid state due to dipole-dipole interaction[27]. Such interaction is not detected when the complex is dissolved in DMSO. The parameter (G), gives information about exchange interaction between copper centers in polycrystalline state[28]. The obtained G value of this complex is 2.25. This value ($G < 4$) suggests that there is an exchange interaction between the copper centers in **1**[29]. These epr behaviour of **2** in polycrystalline is most likely caused by spin-exchange between paramagnetic copper centers. A frozen solution epr spectrum of this complex is consistent with the monomeric structure and found a trend in the spin Hamiltonian parameters ($g_{\parallel} > g_{\perp} > 2.0023$) and $A_{\parallel} \simeq 156 \times 10^{-4}$ cm^{-1} indicates a $d_{x^2-y^2}$ ground state with tetragonal symmetry for copper(II).[5] Half-field signal was not detected in frozen solution epr spectra.[29] The observed $g_{\parallel}$ value for this complex is 2.202 which is less than 2.3 indicates a covalent environment[30].

Polycrystalline RT spectrum of polynuclear complex **2** is quite different in appearance than complex **1**. A weak half-field signal (~1500 G) is observed at the $g \cong 4.37$, which is associated with the $\triangle M_s = \pm 2$ transitions from a coupling between $s = {}^1/_2$ metal ions, in a molecule (intra dipole-dipole interaction). Such epr spectral behavior suggests that the two copper centers are coupled antiferromagnetically as evidenced by magnetic susceptibility measurements. Additionally, parameter G yielded G = 3.00, suggesting interaction in a polycrystalline state which may be propagated through $[^{Cu-N}\!\!\bigcirc\!\!^{N-Cu}]^{n+}$ core.[31] Frozen solution epr spectrum of **2** consistent with monomeric structures. Obviously, DMSO causes the dissociation of the polynuclear complex into a mononuclear complex responsible for the doublet spectrum and probably, a dinuclear species, although the half-field signal is not detected in the frozen solution epr spectrum.

Electrochemistry

The electrochemical behaviour of the complexes was studied using CV and DPV in DMSO solution (3×10^{-3} M). The cyclic and differential pulse voltammograms are displayed in Fig. 4 and electrochemical data are presented in Table 4. The conductivity values were found to be 235 and 211 Ω^{-1} mol^{-1} cm^2 for **1** and **2**, respectively. This indicates that both the complexes are 1:2 type electrolytes[32].

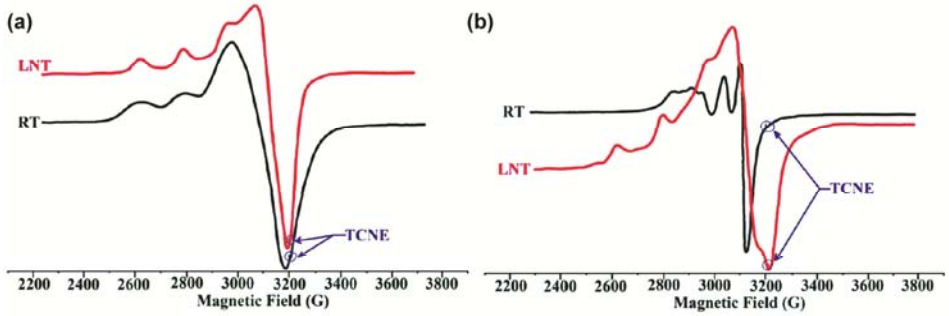

Fig. 3 — Epr spectra of complexes (a) **1** and (b) **2**

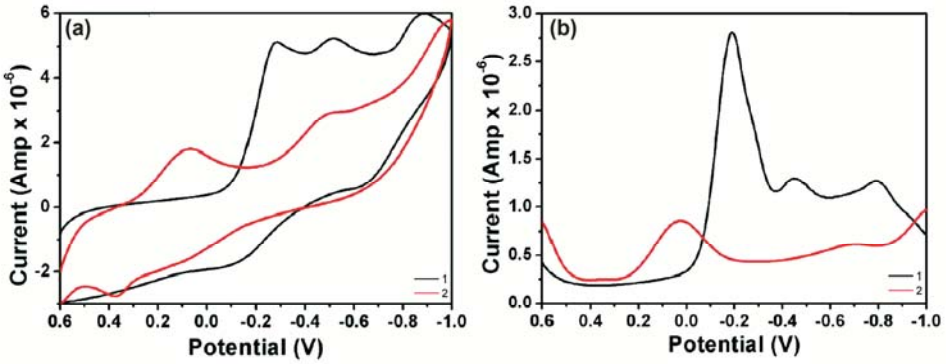

Fig. 4 — (a) CV and (b) DPV plots of complexes **1** and **2** in DMSO (3.0×10^{-3}M) solution

The CVs of both complexes displayed two distinct reduction and oxidation waves. These two one electron reduction waves correspond to $Cu^{II}Cu^{II} \rightleftharpoons Cu^{II}Cu^{I} \rightleftharpoons Cu^{I}Cu^{I}$ process[33]. The observed extra peak at more negative potential may be due to the reduction of ligand moiety. Such findings are indicative of significant metal coupling for both complexes[34] and reduction potential found for **1** and **2** are in agreement reported in the literature[35].

The observed couples are irreversible with peak separation ~0.684 V. The stability of mixed-valence $Cu(II) - Cu(I)$ species increases with increasing ligand instauration and can be expressed in terms of the conproportionation constant k_{con}[36]. The larger the separation between the peak potentials of the couple, the greater is the stability of the mixed-valence species with respect to conproportionation. The values of ΔE and k_{con} are presented in Supplementary Data, Table S3. The k_{con} of **1** was found 9.7×10^3 compared to the value ofk_{con} 9.6×10^4 for **2** suggesting that **2** is more stable.

UV-visible absorption spectra

The absorption spectra of both complexes were recorded in DMSO (1×10^{-3} M). The light green coloured complex **1** displays two peaks centered at 652 nm with a shoulder at 922 nm. The spectrum of **2** also displayed a broad *d-d* band consisting of two peaks centered at 620 nm and shoulder at 976 nm (Fig. 5). The ligand to the metal charge transferred (MLCT) ~425 nm and π-π^* ~352 nm due to ligand only are also observed[37]. The extinction coefficient (ε) of *d-d* bands are in the range of 620-976 M^{-1} cm^{-1}. Such a low value of ε suggests the *d-d* nature of the transition from the low-lying filled d-orbital to the upper-filled orbital[38].

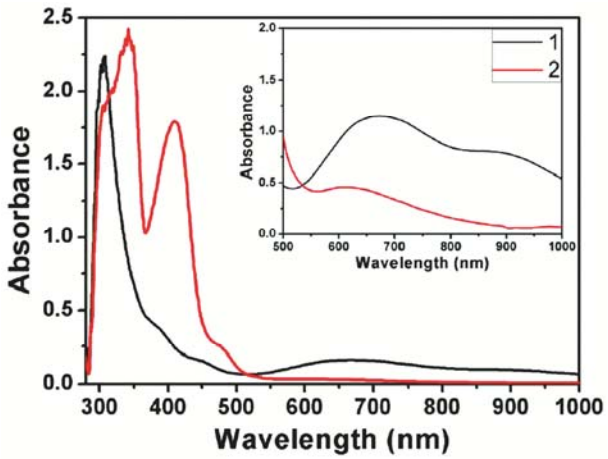

Fig. 5 — Absorption spectra (zoomed region from 500–1000 nm is shown in inset for clear visibility)) of 1×10^{-3} M DMSO solution of complexes **1** and **2**

Computational studies

Orbital analysis

The ground-state electronic structures of the present complexes are computed to obtain further insight into the electronic structures (atomic arrangement) of complexes. The computed features of frontier molecular orbital (FMO) is in terms of energies, the present composition of the ligand and metal orbitals and the contribution of used different ligands are listed in Table 2 and shown in Fig. 6. The highest occupied molecular orbitals (HOMO) are in general assigned by the π-orbitals of proligand (Schiff base) whereas the lowest occupied molecular orbitals (LUMO) are devoted by π^* ligands.

Global chemical reactivity

Different quantum chemical parameters obtained from DFT strategies which were estimated to explain the stability and reactivity of complexes (**1** and **2**). The calculated parameters reveal energies of HOMO and LUMOs (E_{HOMO} and E_{LUMO}), the energy gap (ΔE),

electronegativity (χ), chemical potential (P_i), global hardness (η), global softness (σ), global electrophilicity index (ω) and additional electronic charge (ΔN_{max})[39]. The value electronegativity (χ) is estimated by using $\chi = IP + EA/2$. Similarly $\eta = IP - EA/2$ and S = ½.[40] The ΔE between FMOs indicating HOMO and LUMO energies indicating the electron-donating and accepting capability describes spectroscopic features of the molecules, molecular chemical stability chemical reactivity. During the complex formation, metal behaves as a Lewis acid (electron acceptor) and ligand acts as an electron as a Lewis base (electron donor). The chemical reactivity of a complex molecule is a function of HOMO and LUMO of the different reacting species[41]. Estimated values of ΔE, global softness and chemical potential also support this suggestion. Absolute hardness (η) and softness (S) are important properties to evaluate the molecular stability and reactivity. The greater the ΔE, the higher is the stability of the complexes. On the basis of the data in Table 2, it can be said that the complexes are stable transition metal complexes[42]. The evaluated ΔE of 211 revealed that the Cu^{2+} complex has the lower ΔE, which is indicative of more probable complex formation.

Natural bond Order (NBO) calculations

The NBO calculations were made at the B3LYP/LANL2DZ level of theory[43]. NBO calculations reveal a closer insight into the effect of single donors participating in the coordination sphere of the transition metal complexes. They permit the correlation between structural features and electrochemical properties of complexes. Values of NBO analysis for the complex **1**, the electronic arrangement of the copper atom is: [Ar] 4s (0.23) 3d (9.76) 4p (0.38) 5p (0.01). The 17.994 core electrons, 10.376 valence electrons and 0.012 Rydberg electrons, which yields a sum of 28.382 electrons and +0.617 charge on copper atom (Table 3). This is in concurrence with the natural charge of the copper atom (+0.617), which agrees with the difference between 28.382 and the total number of electrons in an isolated copper atom (29e). Similarly, the core, valence, Rydberg electrons and natural charge on copper atoms of complex **2** have also been calculated and collected in Table 4. The formal charges of donor atoms of ligands reveal that the electron distribution is not limited to the coordination bonds in between metal and donor atoms as the estimated formal charges of Cu (0.619) is smaller than +2. Such a lower charge value is presumed upon complex

Table 2 — Calculated quantum chemical parameters

Compound	E_{HOMO}	E_{LUMO}	ΔE	χ	η	σ	ω	P_i	ΔN_{max}
1	-3.291	-0.419	2.872	1.855	0.927	0.539	1.855	-1.855	2.001
2	-2.241	-2.102	0.139	2.171	0.069	7.246	34.152	-2.171	31.463

Table 3 — Natural electron configuration of copper(II) complexes

Complex	Natural electronic configurations					Core	Valence	Rydberg
		4s	3d	4p	5p			
1	Cu(1)	0.23	9.76	0.38	0.01	17.994	10.376	0.012
2	Cu(2)	0.28	9.29	0.58	0.01	17.994	10.143	0.014

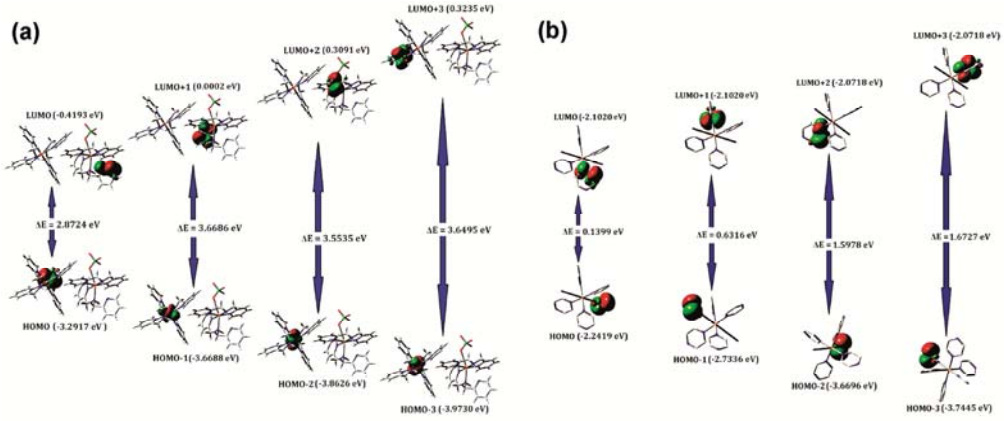

Fig. 6 — Frontier molecular diagram of complexes (a) **1**, and (b) **2**

formation with charge transfer from the metal (copper) centers to the ligand.

Hirshfeld surface analysis

Molecular Hirshfeld surfaces[44] in the crystal structures of **1** and **2** were constructed on the basis of the electron distribution calculated as the sum of spherical atom electron densities[45]. For a given crystal structure and a set of spherical atomic densities, the Hirshfeld surface is unique[46]. The normalized contact distance (d_{norm}) based on both d_e and d_i (where d_e is the distance from a point on the surface to the nearest nucleus outside the surface and d_i is the distance from a point on the surface to the nearest nucleus inside the surface) and the vdW radii of the atom, as given by Eqn. (3) enables identification of the regions of particular importance to intermolecular interactions.[44] The combination of d_e and d_i in the form of two-dimensional (2D) fingerprint plot[47] provides a summary of intermolecular contacts in the crystal[44]. The Hirshfeld surfaces mapped with d_{norm} and 2D fingerprint plots were generated using the Crystal-Explorer 2.1[48]. Graphical plots of the molecular Hirshfeld surfaces mapped with d_{norm} used a red-white-blue colour scheme, where red highlight shorter contacts, white represents the contact around vdW separation, and blue is for longer contact. Additionally, two further coloured plots representing shape index and curvedness based on local curvatures are also presented in this paper[49].

$$\boldsymbol{d_{norm}} = \frac{\boldsymbol{d_i - r_i^{vdW}}}{\boldsymbol{r_i^{vdW}}} + \frac{\boldsymbol{d_e - r_e^{vdW}}}{\boldsymbol{r_e^{vdW}}} \quad ...(3)$$

The Hirshfeld surfaces for complexes **1** and **2** are presented in Fig. 7. The d_{norm} surface has been mapped over a range of -0.5 to 1.5 Å while shape index and curvedness are mapped over the ranges -1.0 to 1.0 Å and -4.0 to 0.4 Å, respectively. For better visualization of the aromatic rings, chelate rings and other entities in both complexes these surfaces are presented as transparent. The weak interactions discussed in the structural description for all the three complexes are presented effectively in the various spots. In the d_{norm} surfaces, the large circular deep red depressions are indicating hydrogen bonding contacts. The other dominant interaction C−H···π interactions in **1** and O···π interactions in **2** in surface plots are evinced as a faint red shaded area.

The fingerprint plots for the complexes **1** and **2** are shown in Fig. 8. The figure depicts that the complementary regions in plots can be visualized where one molecule behaves as a donor ($d_e > d_i$) while another behaves as an acceptor ($d_e < d_i$). The

Table 4 — The NBO charge of atoms in complexes

Complex	atom	NBO charge	atom	NBO charge
1	Cu1	+0.617	O61	-0.914
	N2	-0.536	O62	-0.860
	N3	-0.744	Cu63	+0.612
	N5	-0.521	N64	-0.478
	N6	-0.558	N65	-0.703
	N7	-0.670	N67	-0.515
	N9	-0.544	N68	-0.516
	Cl58	+2.613	N69	-0.913
	O59	-0.893	N70	-0.506
	O60	-0.850		
2	Cu1	+0.847	N25	-0.506
	N2	-0.506	N26	-0.506
	N3	-0.599	N27	-0.599
	N9	-0.433	N32	-0.433
	N14	-0.449	N41	-0.433
	N15	-0.506	N47	-0.449
	N20	-0.433		

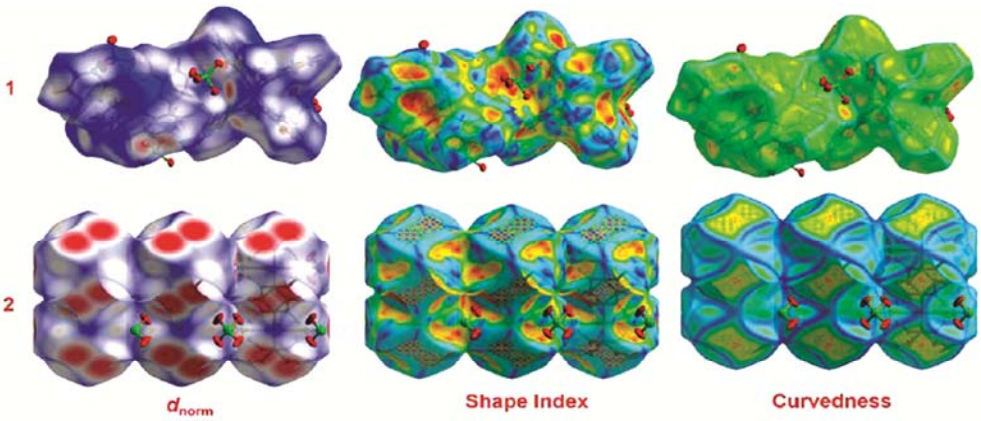

Fig. 7 — Hirshfeld surfaces mapped with d_{norm}, shape index and curvedness for complexes **1** and **2**

fingerprint plots for both the complex don't possess spikes of equal lengths. Also, the peculiar fingerprint plot associated with **2** is because of its polymeric characteristics. The O···H interactions complex **1** appears as two distinct spikes of unequal width while in the case of **2** it appears as a single spike of wavy character in their corresponding decomposed 2D fingerprint plots. The fingerprint plots can be split apart to highlight particular atom pair close contacts. This enables the separation of contributions from different interaction types, which overlap in the full fingerprint. In **1**, O···H interactions appears in the region 1.0 Å < (d_e + d_i) < 2.6 Å whereas in **2** it arises in the region 1.0 Å < (d_e + d_i) < 2.6 Å (for **2**) as light sky-blue pattern. In **1**, C-H···π interaction area covers relatively more area than O···H which ranges in the region 0.5 Å < (d_e + d_i) < 2.8 Å, while, in **2**, the O···π interactions appear at the upper region in the fingerprint plot in the region 1.8 Å < (d_e + d_i) < 2.8 Å. The proportions of O···H interactions constitute 38.7% and 44.5% of their total Hirshfeld surfaces in **1** and **2**, respectively. The C-H···π interactions in **1** and O···π interactions in **2** exhibit contributions of 19.5% and 8.3% in their respective total Hirshfeld surfaces.

Antibacterial activity studies

The antibacterial actions of the complexes **1** and **2** were screened on one gram-positive (*Staphylococcus aureus*) and two gram-negative (*E. coli* and *Proteus vulgaris*) bacteria by diffusion disk technique[14]. The results of antibacterial activity are collected in Table S4 and the effects of the complexes on the growth are shown in Fig. 9. It is clear from this figure that the growth inhibitions are smaller than control (tetracycline). The antibacterial activity of complexes could be explained on the basis of chelation theory[50]. Both complexes show enhanced activity against *E.coli* and *Proteus vulgaris* (gram-negative) than *S. aureus* (gram-positive bacteria). Complex **2** is highly active against *E. coli*.

Antioxidant superoxide dismutase (SOD) activity

SOD activity of both complexes was explored using the alkaline DMSO (NBT) assay method (Fig. 10). In this method, superoxide anion (O_2^-)

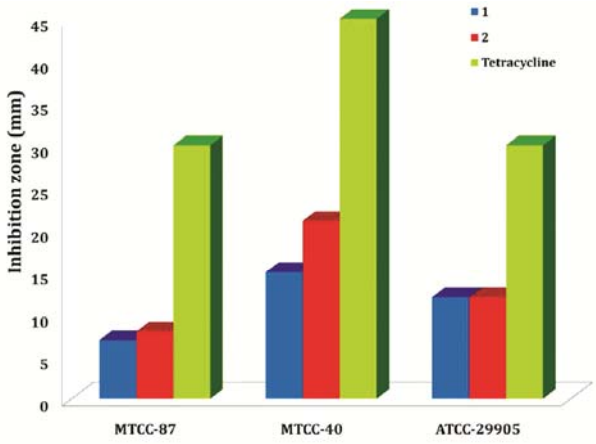

Fig. 9 — Biological activity of the complexes **1** and **2**

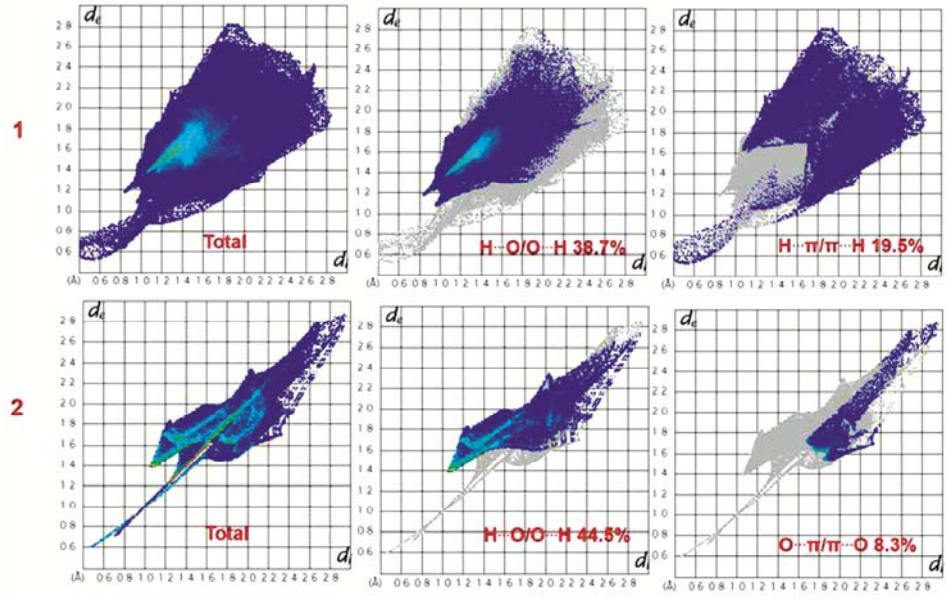

Fig. 8 — Fingerprint plots for complexes **1** and **2** showing percentages of contact contributed to the total Hirshfeld surface area of the molecules

originated by the alkaline DMSO reduces yellow NBT to the blue formazan (MF^-) and magnitude of $MF^+$is measured spectrophotometrically at 560 nm. The alkaline DMSO allows the generation of a large amount of O_2^- which is stable in solution. Therefore, the compound can compete with NBT for the oxidation of the generated O_2^-. Scavengers can inhibit the formation of blue formazan. SOD activity (IC_{50}) along with other parameters are shown in Table 5. The measured IC_{50} values of both complexes exhibit catalytic activity towards dismutation of O_2^-. SOD data of other mononuclear SOD mimics are also given in the table for comparison points of view[51-53]. Both complexes exhibited moderate SOD activity value. The moderate SOD activity of these complexes can be explained by considering a possible correlation between the strength of the equatorial field and the superoxide activity[54]. The SOD value of complex **1** is more than **2**. The SOD activity of present complexes was significantly higher than vitamin C (control). Probably the observed difference in SOD data could be due to different molecular structures in complexes **1** and **2**. The proposed catalytic mechanism could be in the following two steps (Scheme 2). In step (i), an inner-sphere electron transfer occurs between the coordinated superoxide and copper-ligand bond is assisted due to protonation by the solvent and oxygen molecule. In step (ii), reoxidation of Cu^+ to Cu^{2+} by the next O_2^- happened with the transfer of a proton to the hydroperoxide ion[55].

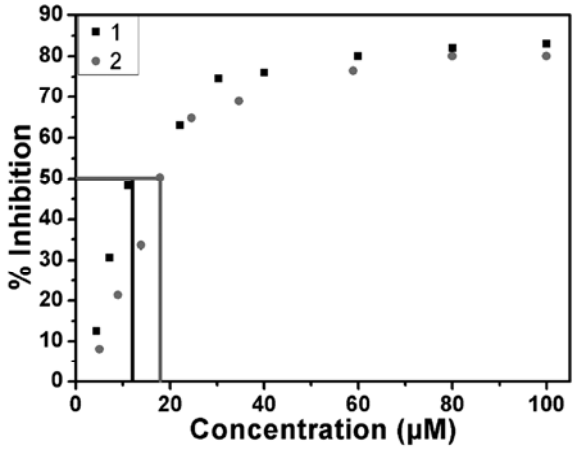

Fig. 10 — Plot of % inhibition of NBT reduction vs concentration of complexes **1** and **2**

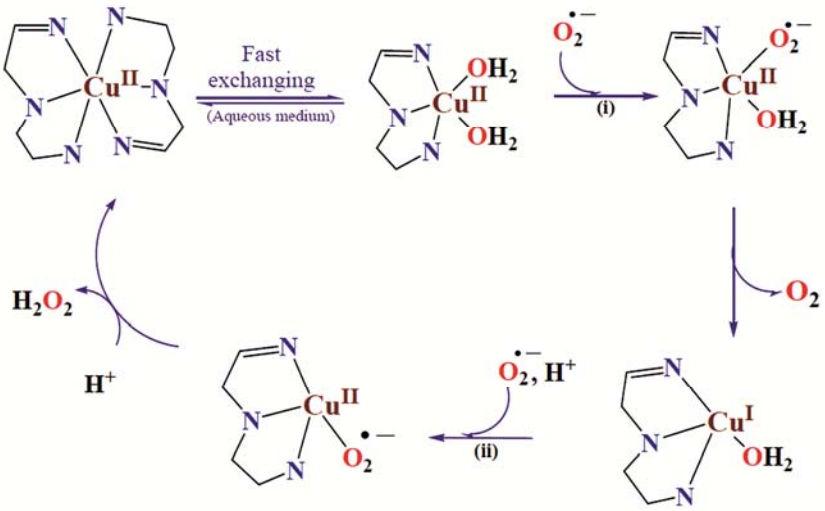

Scheme 2 — Suggested mechanism of O_2^- dismutation reaction catalyzed by the complex

Table 5 — SOD activity data of complexes

S. No.	Complex	IC_{50}(μM)	SOD Activity (μM^{-1})	k_{M_cCF} $(mol\ L)^{-1}\ s^{-1} \times 10^4$	Reference
1	$[Cu(salicylate)_2]$	16	16.50	20.79	51
2	$[Cu(acetyl\ salicylate)_2]$	23	43.48	14.36	51
3	$[Cu(L^1)(H_2O)(NO_3)]H_2O$	8	125.00	41.58	52
4	$[Cu(L^1)(H_2O)(NO_3)$	6	166.67	55.44	52
5	Vc	852	1.17	0.39	53
6	$[Cu_2(DPA)_4(ClO_4)].3ClO_4$	13	76.92	25.58	This work
7	$[Cu_2(\mu\text{-pyrz})(2\text{-pyrz})_3].4ClO_4$	18	55.55	18.48	This work

Conclusions

In summary, we have synthesized and characterized two new copper(II) complexes of $[Cu(DPA)_4](ClO_4)_2$ (**1**) and $[Cu_2(\mu\text{-}pyrz)(pyrz)_3](ClO_4)_4$ (**2**). The molecular structures were determined using single crystal X-ray diffraction technique. Structures of both complexes were stabilized by strong hydrogen bondings. The electrochemical behaviour of complexes was studied using cyclic voltammetry and differential pulse voltammetry. Cyclic voltammograms of both complexes revealed two distinct reduction and oxidation waves. X-band epr spectra in frozen solutions with $g_{\parallel} > g_{\perp} > 2.0023$ showing a $d_{x^2-y^2}$ ground state for copper(II). Antibacterial and antioxidant data were also collected for both complexes. Results of SOD activity showed considerable activity and inspire us to work for the development of good SOD mimics.

Supplementary Data

The X-ray crystallographic data for the structures reported in this article have been deposited at the CCDC as supplementary data CCDC No. 2050277 (**1**) and 2050278 (**2**). These data can be obtained free of charge via https://summary.ccdc.cam.Ac.uk/structure-summary-from the Cambridge Crystallographic Data Center, 12 Union Road, Cambridge CB2 1EZ, UK; E-mail: deposit@ccdc.cam.ac.uk. Supplementary data associated with this article are available in the electronic form at http://nopr.niscair.res.in/jinfo/ijca/IJCA_60A(04)506-518_SupplData.pdf.

Acknowledgement

The authors are thankful to the Council of Scientific and Industrial Research (CSIR), New Delhi, India (Grant No. 01(2917)/18/EMR-II) for funding this research and to RSIC (SAIF), Indian Institute of Technology Bombay, for EPR measurements.

References

1 Vigato P A, Tamburini S & Fenton D E, *Coord Chem Rev*, 106 (1990) 25.
2 McKee V, Zvagulis M, Dagdigian J V, Patch M G & Reed C A, *J Am Chem Soc*, 106 (1984) 4765.
3 Cass A E G, *Superoxide dismutases in Metalloproteins*, vol. 1, chapter 4, Harrison P M (Ed.), (Verlog Chemie, Basol) 1985, p. 121.
4 Riley D P, *Chem Rev*, 99 (1999) 2573.
5 Gagne R R, Koval C A, & Lisensky G C, *Inorg Chem*, 19 (1980) 2854.
6 Sheldrick G M, *Acta Crystallogr Sect A: Found Crystallogr*, A46 (1990) 467.
7 Sheldrick G M, *Acta Crystallogr Sect C*: *Cryst Struct Commun*, C71 (2015) 3.
8 Spek A L, *Acta Crystallogr Sect D: Biol Crystallogr*, D65 (2009) 148.
9 Farrugia L J, *J Appl Crystallogr*, 45 (2012) 849.
10 Sheldrick G M, *Acta Crystallogr Sect A: Found Crystallogr*, A64 (2008) 112.
11 Murray P R, Baron E J, Pfaller M A, Tenover F C & Yolke R H, *Manual of Clinical Microbiology*, 6th edition (American Society of Microbiology Press, Washington DC) 1995.
12 Kumar K & Murugesan S, *J Soudi Chem Soc*, 22 (2018) 16.
13 Patel R N, Singh A, Shukla K K, Patel D K & Sondhiya V P, *J Coord Chem*, 64 (2011) 902.
14 Liao Z R, Zheng X F, Luo B S, Shen L R, Li D F, Liu H L & Zhao W, *Polyhedron*, 20 (2001) 2813.
15 Petersson G A & Al-Laham M A, *J Chem Phys*, 94 (1991) 6081.
16 Hay P J & Wadt W R, *J Chem Phys*, 82 (1985) 270.
17 Frisch M J, Trucks G W, Schlegel H B, Scuseria G E, Robb M A, Cheeseman J R, Scalmani G, Barone V, Mennucci B, Petersson G A, Nakatsuji H, Caricato M, Li X, Hratchian H P, Izmaylov A F, Bloino J, Zheng G, Sonnenberg J L, Hada M, Ehara M, Toyota K, Fukuda R, Hasegawa J, Ishida M, Nakajima T, Honda Y, Kitao O, Nakai H, Vreven T, Montgomery Jr J A, Peralta J E, Ogliaro F, Bearpark M, Heyd J J, Brothers E, Kudin K N, Staroverov V N, Kobayashi R, Normand J, Raghavachari K, Rendell A, Burant J C, Iyengar S S, Tomasi J, Cossi M, Rega N, Millam J M, Klene M, Knox J E, Cross J B, Bakken V, Adamo C, Jaramillo J, Gomperts R, Stratmann R E, Yazyev O, Austin A J, Cammi R, Pomelli C, Ochterski J W, Martin R L, Morokuma K, Zakrzewski V G, Voth G A, Salvador P, Dannenberg J J, Dapprich S, Daniels A D, Farkas O, Foresman J B, Ortiz J V, Cioslowski J & Fox D J, *Gaussian 09, Revision* D 01, (Gaussian Inc, Wallingford CT) 2009.
18 Bauernschmitt R & Ahlrichs R, *Chem Phys Lett*, 256 (1996) 454.
19 Cossi M, Rega N, Scalmani G & Barone V, *J Comput Chem*, 224 (2003) 669.
20 Mosmann T, *J Immunol Methods*, 65 (1983) 55.
21 Ghosh K, Kumar P, Tyagi N, Singh U P, Aggarwal V & Baratto M C, *Eur J Med Chem*, 45 (2010) 3770.
22 Murthy P R & Patel C C, *Can J Chem*, 42 (1964) 856.
23 Singh Y P, Patel R N & Singh Y, *Indian J Chem*, 57A (2018) 44.
24 Addison A W, Rao T N, Reedjik J, Rijn J V & Verschoor C G, *J Chem Soc Dalton Trans*, (1984) 1349.
25 Karlin K D, Hayes J C, Juen S, Hutchinson J P & Zubieta J, *Inorg Chem*, 21 (1982) 4106.
26 Scott B, Geiser U, Willett R D, Patyal B, Landee C P, Greeney R E, Manfredini T, Pellacani G C, Corradi A B & Battaglia L P, *Inorg Chem*, 27 (1988) 2454.
27 Kahn O, *Molecular Magnetism*, (Wiley VCH, New York) (1993).
28 Patel R N, Singh Y P, Singh Y, Butcher R J & Jasinski J P, *Polyhedron*, 129 (2017) 164.
29 Hathaway B J & Billing D E, *Coord Chem Rev*, 5 (1970) 143.

30 Kivelson D & Neiman R, *J Chem Phys*, 35 (1961) 149.
31 Patel R N, Singh Y P, Singh Y, Butcher R J & Zeller M, *RSC Adv*, 6 (2016) 107379.
32 Geary W J, *Coord Chem Rev*, 7 (1971) 81.
33 Ohtsu H, Shimazaki Y, Odani A, Yamauchi O, Mori W, Itoh S & Fukuzumi S, *J Am Chem Soc*, 122 (2000) 5733.
34 Belle C, Beguin C, Gautier–Luneau I, Hamman S, Philouze C, Pierre J L, Thomas F, Torelli S, Saint–Aman E & Bonin M, *Inorg Chem*, 41 (2002) 479.
35 Osório R E H M B, Peralta R A, Bortoluzzi A J, de Almeida V R, Szpoganicz B, Fischer F L, Terenzi H, Mangrich A S, Mantovani K M, Ferreira D E C, Rocha W R, Haase W, Tomkowicz Z, dos Anjos A & Neves A, *Inorg Chem*, 51 (2012) 1569.
36 Gervasio G, Rossetti R, Stanghellini P L & Bor G, *J Chem Soc Dalton Trans*, (1983) 1613.
37 Lu Y, Roe J A, Bender C J, Peisach J, Banci L, Bertini I, Gralla E B & Valentine J S, *Inorg Chem*, 35 (1996) 1692.
38 Hathaway B J, *Comprehensive Coordination Chemistry*, vol. 5, Wilkinson G, Gillard R D, McCleverty J A (Eds), (Pergamon Press, Oxford, U K) 1987, p. 668.
39 Altürk S, Avcı D, Tamer O, Atlay Y & Şahin O, *J Phys Chem Solid*, 98 (2016) 71.
40 Koopmans T, *Physica*, 1 (1934) 104.
41 Fuki K, *Science*, 218 (1982) 747.
42 Soliman A A, Amin M A, Sayed A M, Abou-Hussein A A A, Linert W, *Polyhedron*, 161 (2019) 213.
43 Reed A E, Curtius L A, Weinhold F, *Chem Rev*, 88 (1988) 899.
44 Spackman M A & McKinnon J J, *CrystEngComm*, 4 (2002) 378.
45 McKinnon J J, Mitchell A S & Spackman M A, *Chem Eur J*, 4 (1998) 2136.
46 McKinnon J J, Spackman M A & Mitchell A S, *Acta Crystallogr Sect B : Struct Sci, Cryst Eng Mater*, B60 (2004) 627.
47 Rohl A L, Moret M, Kaminsky W, Claborn K, McKinnon J J & Kahr B, *Cryst Growth Des*, 8 (2008) 4517.
48 Wolff S K, Greenwood D J, McKinnon J J, Jayatilaka D & Spackman M A, *Crystal Explorer 2.0*, University of Western Australia, Perth, Australia, 2007.
49 Koenderink J J & van Doorn A J, *Image Vision Comput*, 10 (1992) 557.
50 Bermejo E, Carballo R, Castiñeiras A, Domínguez R, Maichle-Mossmer C, Strähle J & West D X, *Polyhedron*, 18 (1999) 3695.
51 Garriba E & Micera J, *J Chem Educ*, 83 (2006) Article ID 1229.
52 O'Connor C J, *Prog Inorg Chem*, 29 (1982) 203.
53 Li Y, Yang Z-Y, Wu J-C, *Eur J Med Chem*, 45 (2010) 5692.
54 Amar C, Vilkas E, Foos J, *J Inorg Biochem*, 17 (1982) 313.
55 Tainer J A, Getzoff E D, Richardson J S & Richardson D C, *Nature*, 306 (1983) 284.